Pergamon

PII: S0148-9062(98)00015-1

Int. J. Rock Mech. Min. Sci. Vol. 35, No. 6, pp. 771–785, 1998

Printed in Great Britain
0148-9062/98 $19.00 + 0.00

Stress Influence Charts for Transversely Isotropic Rocks

C. D. WANG†
J. J. LIAO†

A graphical procedure to calculate stresses in a transversely isotropic half-space subjected to a three-dimensional surface load has been developed. The surface load can be distributed on an irregularly-shaped area. The planes of transverse isotropy are assumed to be parallel to the horizontal surface of the half-space. The closed-form solutions for stresses at a point under the vertex of a loading sector, with a unit load intensity are presented first. Based on these solutions, five influence charts are constructed for calculating the six components of a stress tensor at any given point in the half-space. The charts are composed of unit blocks. Each unit block is bounded by two adjacent radii and arcs, and contributes the same level of influence to the stress within the half-space. An example is presented to demonstrate the use of the new graphical method. For the case analyzed, results from the new graphical method agree with those of analytical solutions within 3%. The new influence charts can be a practical alternative to the existing analytical or numerical solutions, and provides results with reasonable accuracy. © 1998 *Elsevier Science Ltd.*

INTRODUCTION

Anisotropy in deformability is common for foliated metamorphic, stratified sedimentary, and regularly jointed rock masses. Existing analytical solutions based on linear and isotropic elasticity for stress analyses in these types of rocks or rock masses are only rough approximations. To obtain more desirable results, it is imperative to consider the anisotropic deformability.

There have been several reports [1–3] on the closed-form solutions of displacements and stresses due to a point load for a transversely isotropic half-space. Solutions other than point load conditions, however, are limited. Elastic solutions for displacements or stresses in a half-space, subjected to loads of regular shapes, (e.g., line loads [4–6], rectangular loads [6], triangular loads [7], circular loads [4, 8–14], parabolic loading over a circular region [12, 15–17], ring loads [18, 19], elliptical loads [20, 21]), and other related problems [22–25] have also been proposed. These solutions are only applicable to loading of specific and/or regular geometric patterns. It is possible to estimate the stresses and displacements due to an arbitrarily-shaped loading. The loading area is divided into many regularly-shaped sub-areas; influences from these sub-areas are then superimposed. However, the process of superposition is tedious and inconvenient.

†Department of Civil Engineering, National Chiao Tung University, 1001 TA Hsueh Road, Hsinchu, Taiwan, R.O.C.

With the advances in high-speed computers, numerical techniques have been developed for calculating the stresses underneath an irregularly-shaped foundation in the past few decades. These developments include the techniques of equivalent area [26], three-dimensional finite element [27], triangulating [28–31], computer-aided graphics [32], parametric mapping [33], and methods using a packaged software such as MathCAD [34, 35]. Through the use of computer, these methods can easily be automated and hence can be efficient to use.

A graphical method for general shapes of loaded area was first devised by Burmister [36]. That method provided the basis of the Newmark's influence charts [37–39]. The influence charts are efficient to use in calculating stress/displacement as compared to other complex mathematical or numerical methods. However, the advantages of Newmark's charts diminish if the loading area is not uniform or stresses at multiple depths are required simultaneously. Salas [40] proposed modified influence charts. This method is not practical because it involves the use of a table for calculating stress, which is complicated and tedious. Several extensions of the Newmark's method are available. Barber [41, 42] and Barksdale and Harr [43] developed influence charts for the vertical stress due to horizontal shear loading. Huang [44] constructed diagrams for an embedded, distributed uniform vertical load. Poulos [45] proposed a graphical procedure called the sector method. His method can calculate the

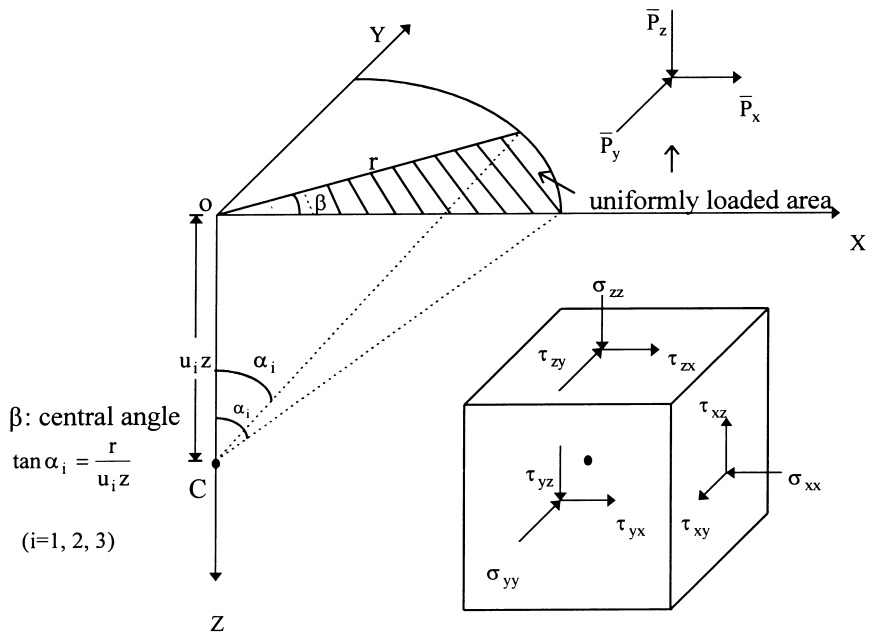

Fig. 1. Uniformly loaded sector area.

displacements and stresses due to any general shape of loaded area.

Applications of the above-mentioned methods are mostly restricted to the stress/displacement evaluation in isotropic media. To the authors' knowledge, no graphical method of stress/displacement calculation has been proposed for a transversely isotropic medium. The aim of this paper is to construct a set of influence

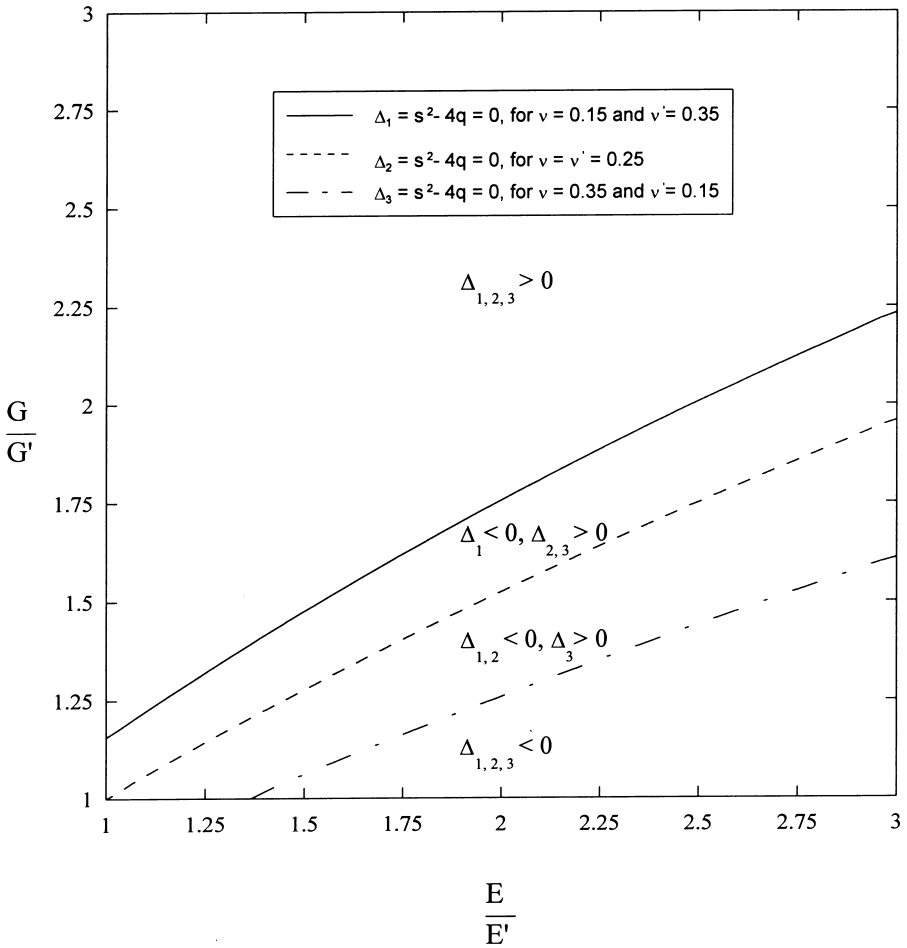

Fig. 2. Distribution of the three types of the characteristic roots for transversely isotropic rocks.

Table 1. Root types of transversely isotropic rocks according to published data

Reference	Material	Test methods	E (GPa)	E' (GPa)	v	v'	G' (GPa)	Root type
Pinto [46]	schist I	uniaxial compression, parallel	95.4	74.5	0.27	0.27	27.2	case 1
	schist II	uniaxial compression, inclined	76.9	41.0	0.22	0.27	20.5	case 1
	schist III	uniaxial compression, inclined	63.4	20.0	0.13	0.21	7.9	case 1
Homand *et al.* [47]	slate	ultrasonic	121.3	58.9	0.19	0.11	15.1	case 1
Liu *et al.* [48]	argillite	uniaxial compression	51.8	32.2	0.19	0.18	13.3	case 1
Amadei [49]	Loveland sandstone I	uniaxial compression	29.3	23.9	0.18	0.13	6.2	case 1
	Loveland sandstone II	uniaxial compression	33.5	44.6	0.08	0.13	19.1	case 3
Liao *et al.* [50]	argillite	direct tension	59.1	51.9	0.22	0.10	14.9	case 1
Liao *et al.* [51]	argillite	ultrasonic	68.3	51.4	0.20	0.16	21.0	case 1

charts analogous to those of Newmark's [38]. The new influence charts are applicable to transversely isotropic media subjected to three-dimensional, arbitrarily-shaped loads. By superposition of values corresponding to the influence charts, the six components of stress tensor at any point in the half-space can be estimated. This paper describes the background of the new influence charts and their application procedure. An illustrative example is presented at the end of the paper to demonstrate the procedure of calculating induced stress using the proposed influence charts. The results are then validated with analytical solutions.

DEFORMABILITY OF TRANSVERSELY ISOTROPIC ROCKS

Anisotropy is a general characteristic of foliated metamorphic rocks (e.g., argillite, slate, schist, phyllite, gneiss), stratified sedimentary rocks (e.g., shale, sandstone, coal, limestone), and regularly jointed rock masses. Deformability anisotropy implies that the deformability of a material is direction dependent. Depending on the planes of elastic symmetry, rock can be of general anisotropy, orthotropy, transverse isotropy, or complete isotropy. Practically, an anisotropic rock can be modelled as either an orthotropic or a

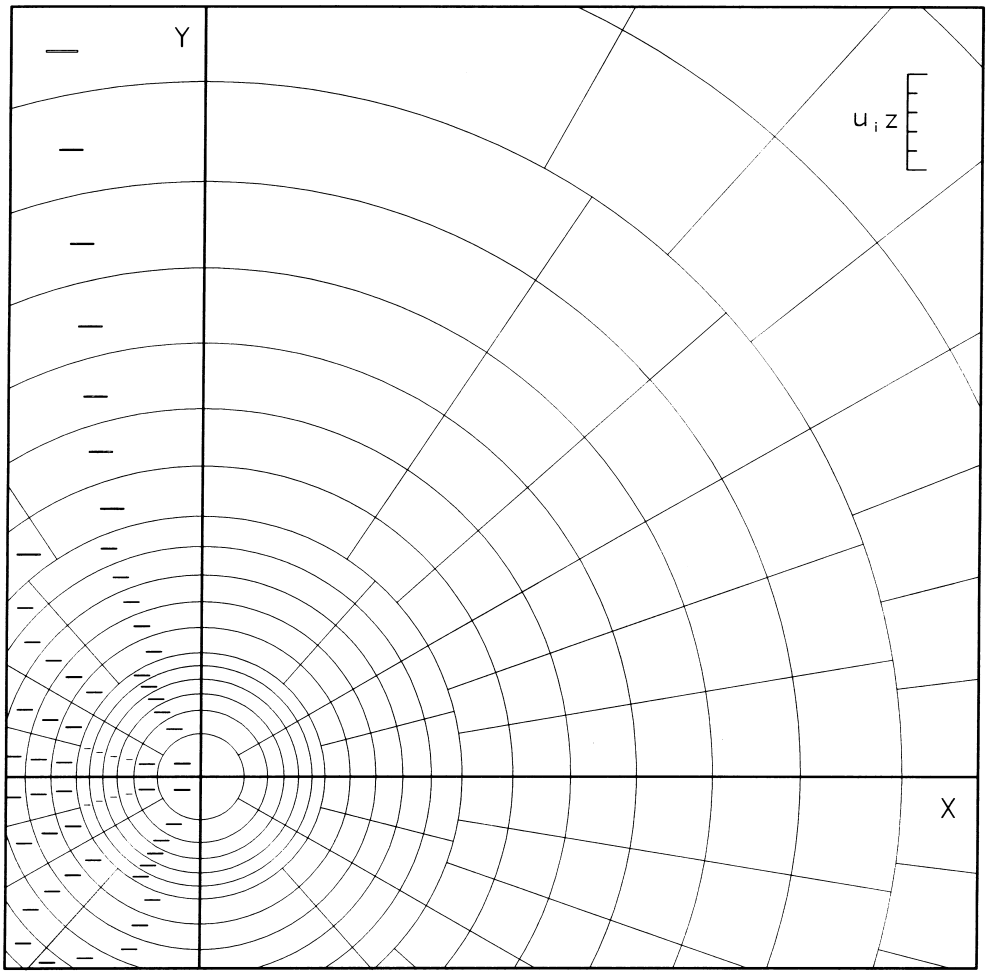

Fig. 3. Influence chart for $a\mathbf{A}_i$ (influence value per block is ± 0.001, negative influences are indicated by a minus, (–), sign).

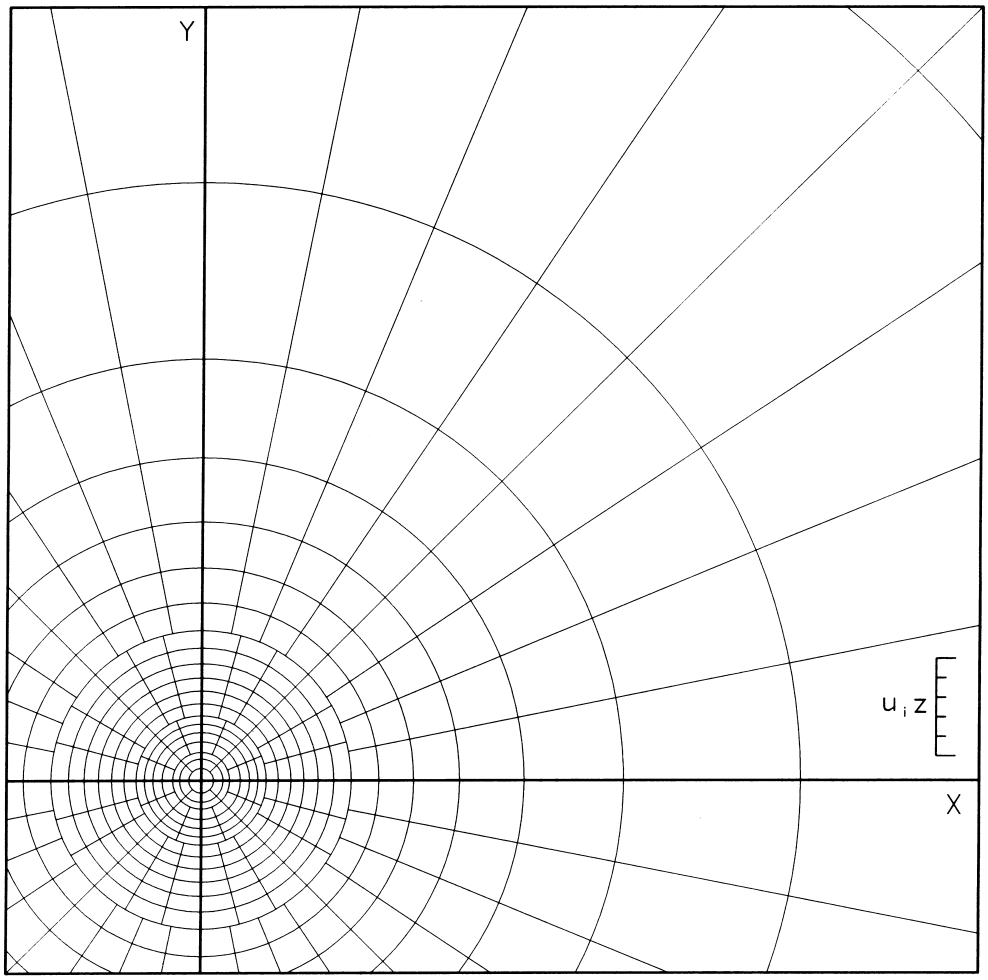

Fig. 4. Influence chart for $c\mathbf{B}_i$ (influence value per block is 0.001).

transversely isotropic material. Orthotropy implies that three orthogonal planes of elastic symmetry exist and that the orientations of these planes remain the same throughout the rock. For a transversely isotropic rock, there is an axis of symmetry of rotation. The rock has isotropic properties in planes normal to this axis. A rock is completely isotropic if it is elastically identical in any direction. The number of elastic constants for describing their deformability is 21, 9, 5, and 2 for generally anisotropic, orthotropic, transversely isotropic, and isotropic rock, respectively. The deformability of a transversely isotropic material can be expressed as the following matrix form, in which the z-axis be the rotation axis of elastic symmetry, x- and y-axes in the plane of transverse isotropy.

$$\begin{bmatrix} \sigma_{xx} \\ \sigma_{yy} \\ \sigma_{zz} \\ \tau_{yz} \\ \tau_{zx} \\ \tau_{xy} \end{bmatrix} = \begin{bmatrix} C_{11} & C_{12} & C_{13} & 0 & 0 & 0 \\ C_{12} & C_{11} & C_{13} & 0 & 0 & 0 \\ C_{13} & C_{13} & C_{33} & 0 & 0 & 0 \\ 0 & 0 & 0 & C_{44} & 0 & 0 \\ 0 & 0 & 0 & 0 & C_{44} & 0 \\ 0 & 0 & 0 & 0 & 0 & C_{66} \end{bmatrix} \begin{bmatrix} \varepsilon_{xx} \\ \varepsilon_{yy} \\ \varepsilon_{zz} \\ \gamma_{yz} \\ \gamma_{zx} \\ \gamma_{xy} \end{bmatrix} \tag{1}$$

where $\sigma_{xx},\sigma_{yy},\sigma_{zz}$ are normal stresses; $\varepsilon_{xx},\varepsilon_{yy},\varepsilon_{zz}$ are normal strains; $\tau_{yz},\tau_{zx},\tau_{xy}$ are shear stresses; $\gamma_{yz},\gamma_{zx},\gamma_{xy}$ are shear strains; C_{11}, C_{12}, C_{13}, C_{33}, C_{44}, C_{66} are elastic constants. The elastic constant C_{12} is equal to $C_{11}-2C_{66}$. Hence, only five elastic constants, i.e., C_{11}, C_{12}, C_{13}, C_{33}, C_{44}, C_{66} are independent for a transversely isotropic material. These constants are directly related to the engineering elastic constants E, E', υ, υ' and G' as follows:

$$C_{11} = \frac{E(1-[(E/E')\upsilon' 2]}{(1+\upsilon)(1-\upsilon-[(2E/E')\upsilon'^2])},$$

$$C_{13} = \frac{E\upsilon'}{1-\upsilon-[(2E/E')\upsilon'^2]},$$

$$C_{33} = \frac{E'(1-\upsilon)}{1-\upsilon-[(2E/E')\upsilon'^2]},$$

$$C_{44} = G',$$

$$C_{66} = \frac{E}{2(1+\upsilon)}$$

where E, E' are the Young's moduli in the plane of transverse isotropy and its normal, respectively; υ, υ' are the Poisson's ratios characterizing the lateral strain

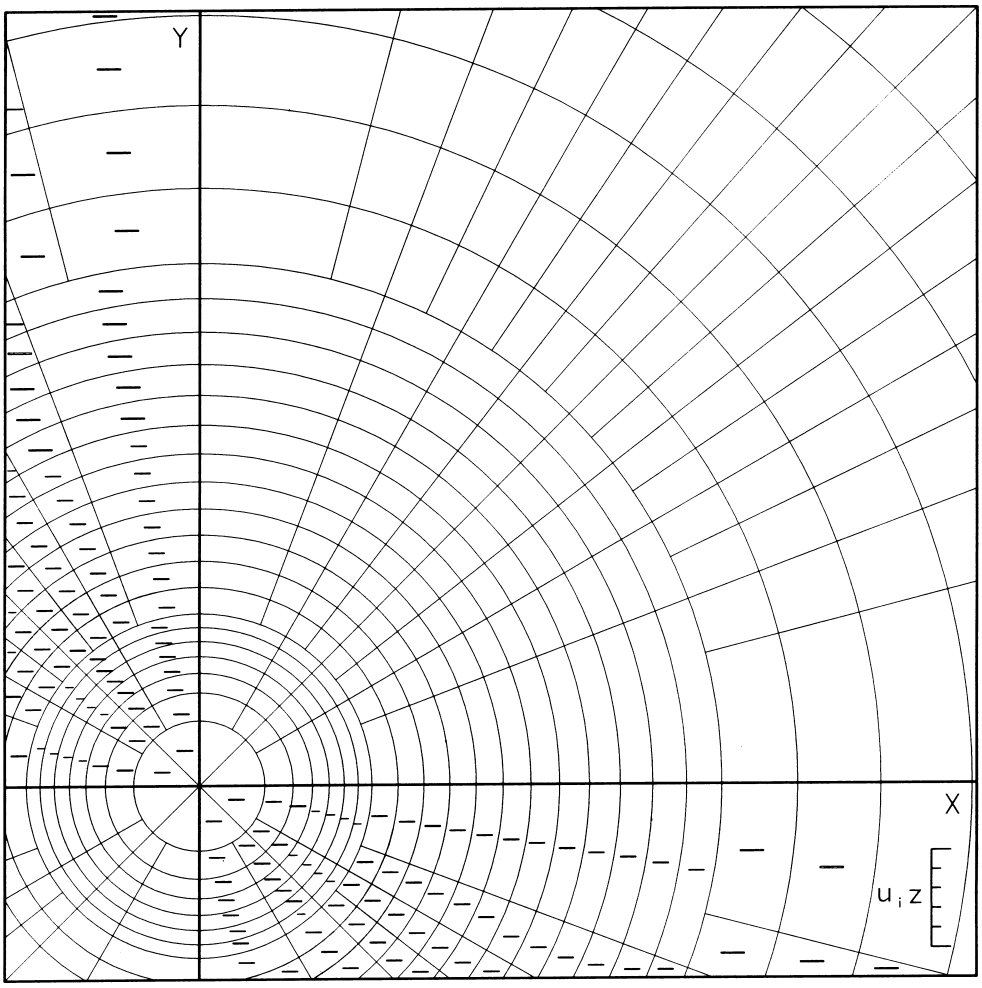

Fig. 5. Influence chart for $d\mathbf{C}_i$ (influence value per block is ± 0.001, negative influences are indicated by a minus, (–), sign).

in the plane of transverse isotropy to a normal stress acting parallel and normal to it, respectively; and G' is the shear modulus in planes normal to the plane of transverse isotropy.

These engineering elastic constants can be determined by static or dynamic experiments in the laboratory. Readers are referred to [46–51] for details of these methods.

CONSTRUCTION OF THE INFLUENCE CHARTS

This paper concentrates on the development of influence charts that calculate the stresses at a point, in a transversely isotropic half-space, subjected to surface loads. Similar to Newmark's charts [38] for isotropic materials, the proposed charts contain unit blocks. Each block is bounded by two radial lines and two adjacent arcs. The radii of the circles relate to the depth of the interested point in the half-space. The influence value of a unit block in stress should be equal and independent of its location in the chart. To facilitate block counting, the plan of the surface load is drawn to a scale that is proportional to the depth of the interested point. The unit blocks are made roughly square. The number of blocks covered by the scaled loaded area is then counted.

Combining the solutions for stresses induced by different sectors with uniform loads (Fig. 1 shows a typical sector), one can obtain the stresses at point C with depth $u_i z$ due to the uniform load on a unit block.

Stresses under the vertex of a uniformly loaded sector of a circle

The solutions of stresses in a transversely isotropic half-space subjected to a point load have been derived by several investigators (e.g. [1–3]). Integrating the point load solutions, one can obtain the stresses in the half-space subjected to a uniform surface load of any irregularly-shaped area. Details of deriving stresses under the vertex of a uniformly loaded sector of a circle in a transversely isotropic half-space, based on the point load solutions by Liao and Wang [3] are described as follows.

Figure 1 depicts a uniform load, $\bar{P}_j$ (force per unit area, $j = x, y, z$) acts on a sector bounded by two radial lines and a circle arc. In the figure, the depth of point $C(0, 0, u_i z)$ under the vertex is $u_i z$, radius of the arc is r, and the central angle is symbol β (positive counterclockwise with respect to x-axis). Consider an elementary area of $r\,\mathrm{d}r\,\mathrm{d}\beta$ in the sector, the stress at point C, $[\sigma]^C$ is derived by integrating the point load

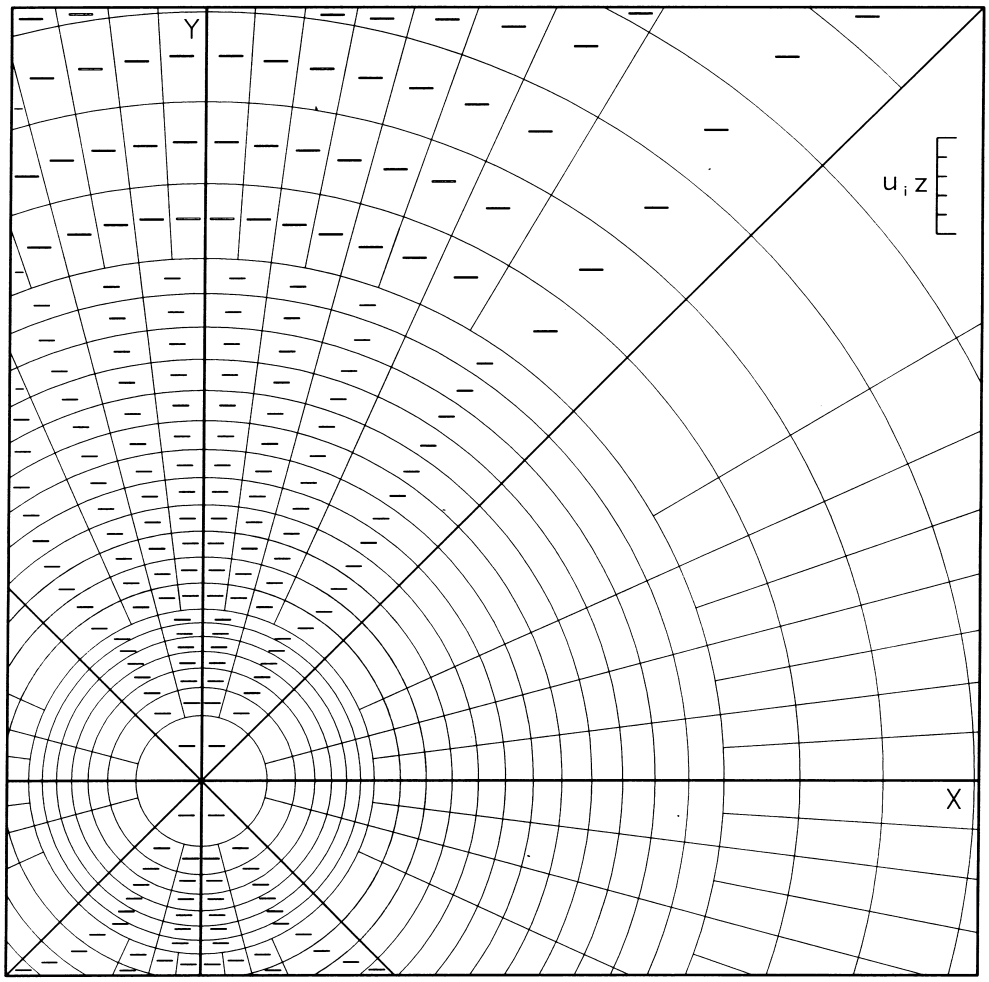

Fig. 6. Influence chart for $e\mathbf{C}_i$ (influence value per block is ± 0.001, negative influences are indicated by a minus, (–), sign).

solutions [3] with dr from 0 to r and dβ from 0 to β [52] as:

$$[\sigma]^C = \int_0^{\beta}\int_0^{r} [\sigma]^{\mathrm{p}} r \, \mathrm{d}r \, \mathrm{d}\beta \tag{2}$$

where $[\sigma] = [\sigma_{xx},\sigma_{yy},\sigma_{zz},\tau_{yz},\tau_{zx},\tau_{xy}]^{\mathrm{T}}$ (superscript T denotes the transpose of matrix); the superscript C denotes the point C at which the induced stresses are evaluated; the superscript p indicates a point load acting at point O. Upon integration, $[\sigma]^C$ has the following components:

$$\begin{aligned}\sigma_{xx}^C = \bar{P}_x\big[&-(4m_1-m_3)\cdot a\mathbf{A}_1 + (4m_2-m_4)\cdot a\mathbf{A}_2 \\ &+ 2u_3\cdot a\mathbf{A}_3 + m_3\cdot f\mathbf{D}_1 - m_4\cdot f\mathbf{D}_2 + 2u_3\cdot fD_3\big] \\ &+ \bar{P}_y\big[-(4m_1-3m_3)\cdot b\mathbf{A}_1 + (4m_2-3m_4)\cdot b\mathbf{A}_2 \\ &- 2u_3\cdot b\mathbf{A}_3 - m_3\cdot g\mathbf{D}_1 + m_4\cdot g\mathbf{D}_2 - 2u_3\cdot gD_3\big] \\ &+ \bar{P}_z\big[-u_2(2m_1-m_3)\cdot c\mathbf{B}_1 + u_1(2m_2-m_4)\cdot c\mathbf{B}_2 \\ &+ u_2m_3\cdot e\mathbf{C}_1 - u_1m_4\cdot e\mathbf{C}_2\big]\end{aligned} \tag{3}$$

$$\begin{aligned}\sigma_{yy}^C = \bar{P}_x\big[&-(4m_1-3m_3)\cdot a\mathbf{A}_1 + (4m_2-3m_4)\cdot a\mathbf{A}_2 \\ &- 2u_3\cdot a\mathbf{A}_3 - m_3\cdot f\mathbf{D}_1 + m_4\cdot f\mathbf{D}_2 - 2u_3\cdot fD_3\big] \\ &+ \bar{P}_y\big[-(4m_1-m_3)\cdot b\mathbf{A}_1 + (4m_2-m_4)\cdot b\mathbf{A}_2 \\ &+ 2u_3\cdot b\mathbf{A}_3 + m_3\cdot g\mathbf{D}_1 - m_4\cdot g\mathbf{D}_2 + 2u_3\cdot gD_3\big] \\ &+ \bar{P}_z\big[-u_2(2m_1-m_3)\cdot c\mathbf{B}_1 + u_1(2m_2-m_4)\cdot c\mathbf{B}_2 \\ &- u_2m_3\cdot e\mathbf{C}_1 + u_1m_4\cdot e\mathbf{C}_2\big]\end{aligned} \tag{4}$$

$$\begin{aligned}\sigma_{zz}^C = {} & 4\bar{P}_x\frac{m_1}{u_1^2}(a\mathbf{A}_1 - a\mathbf{A}_2) + 4\bar{P}_y\frac{m_1}{u_1^2}(b\mathbf{A}_1 - b\mathbf{A}_2) \\ & + 2\bar{P}_z\left(\frac{m_2}{u_2}\cdot c\mathbf{B}_1 - \frac{m_1}{u_1}\cdot c\mathbf{B}_2\right)\end{aligned} \tag{5}$$

$$\begin{aligned}\tau_{yz}^C = {} & \bar{P}_x\left(\frac{m_1}{u_1}\cdot d\mathbf{C}_1 - \frac{m_2}{u_2}\cdot d\mathbf{C}_2 + d\mathbf{C}_3\right) \\ & + \bar{P}_y\left(-\frac{m_1}{u_1}\cdot c\mathbf{B}_1 + \frac{m_2}{u_2}\cdot c\mathbf{B}_2 + c\mathbf{B}_3 - \frac{m_1}{u_1}\cdot e\mathbf{C}_1\right. \\ & \left. + \frac{m_2}{u_2}\cdot e\mathbf{C}_2 - e\mathbf{C}_3\right) + 4\bar{P}_z\frac{u_2m_1}{u_1}(b\mathbf{A}_1 - b\mathbf{A}_2)\end{aligned} \tag{6}$$

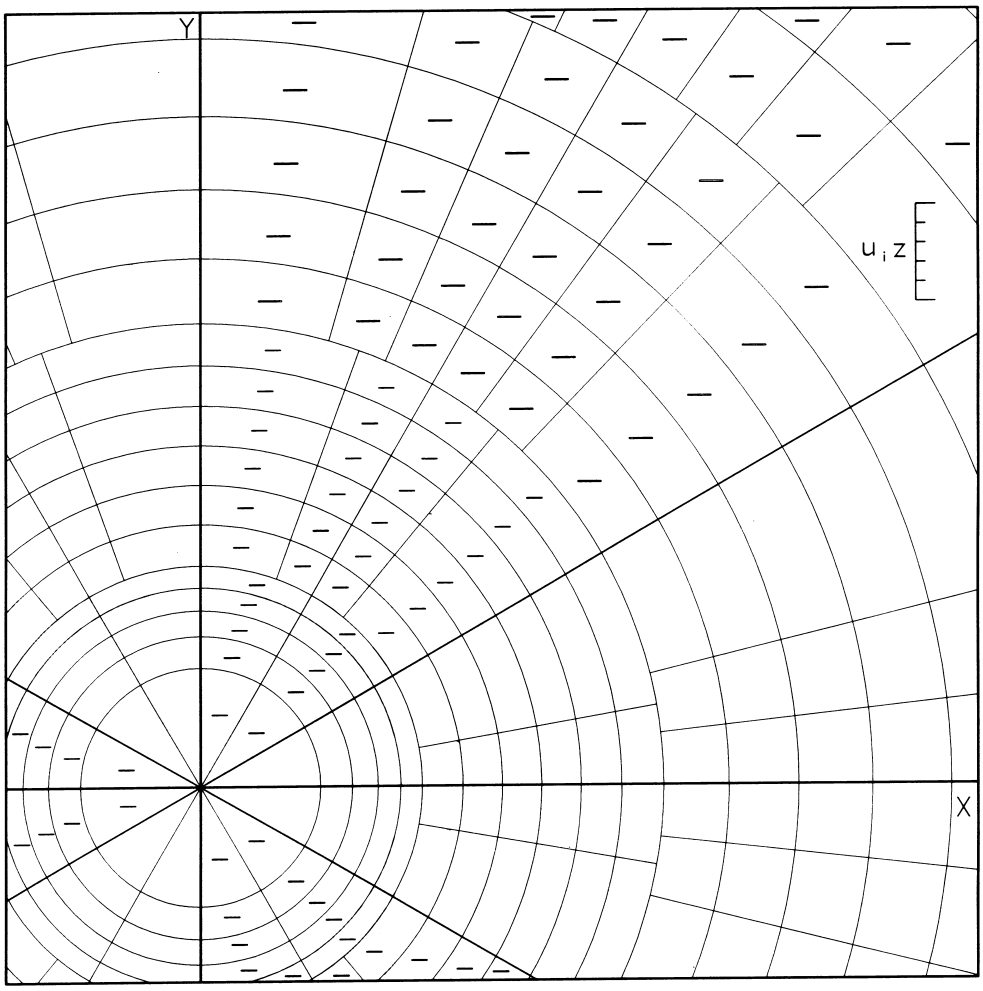

Fig. 7. Influence chart for $f\mathbf{D}_i$ (influence value per block is ± 0.001, negative influences are indicated by a minus, (–), sign).

$$\tau_{xz}^{C} = \bar{P}_x\left(-\frac{m_1}{u_1}\cdot c\mathbf{B}_1 + \frac{m_2}{u_2}\cdot c\mathbf{B}_2 + c\mathbf{B}_3 + \frac{m_1}{u_1}\cdot e\mathbf{C}_1 - \frac{m_2}{u_2}\cdot e\mathbf{C}_2 + e\mathbf{C}_3\right) + \bar{P}_y\left(\frac{m_1}{u_1}\cdot d\mathbf{C}_1 - \frac{m_2}{u_2}\cdot d\mathbf{C}_2 + d\mathbf{C}_3\right) + 4\bar{P}_z\frac{u_2 m_1}{u_1}(a\mathbf{A}_1 - a\mathbf{A}_2) \quad (7)$$

$$\tau_{xy}^{C} = \bar{P}_x(-m_3\cdot b\mathbf{A}_1 + m_4\cdot b\mathbf{A}_2 + 2u_3\cdot b\mathbf{A}_3 - m_3\cdot g\mathbf{D}_1 + m_4\cdot g\mathbf{D}_2 - 2u_3\cdot g\mathbf{D}_3) + \bar{P}_y(-m_3\cdot a\mathbf{A}_1 + m_4\cdot a\mathbf{A}_2 + 2u_3\cdot a\mathbf{A}_3 - m_3\cdot f\mathbf{D}_1 + m_4\cdot f\mathbf{D}_2 - 2u_3\cdot f\mathbf{D}_3) + \bar{P}_z(u_2 m_3\cdot d\mathbf{C}_1 - u_1 m_4\cdot d\mathbf{C}_2), \quad (8)$$

where

$$m_1 = \frac{u_1^2}{u_2 - u_1} \qquad m_2 = \left(\frac{u_2}{u_1}\right)^2 m_1, \quad m_3 = \frac{2u_3^2}{u_1(n+u_1)}m_1,$$

$$m_4 = \frac{n}{u_1}m_3, \qquad n = \frac{(C_{13}+C_{44})u_1}{C_{33}u_1^2 - C_{44}};$$

$$a = \sin\beta, \quad b = 1-\cos\beta, \quad c = \frac{\beta}{2\pi}, \quad d = \frac{1-\cos 2\beta}{2},$$

$$e = \frac{\sin 2\beta}{2}, \qquad f = \frac{\sin 3\beta}{3}, \qquad g = \frac{\cos 3\beta - 1}{3};$$

$$\mathbf{A}_i = \frac{1}{8\pi}\left(-\sin\alpha_i + \ln\left|\frac{1+\sin\alpha_i}{\cos\alpha_i}\right|\right), \qquad \mathbf{B}_i = \frac{1-\cos\alpha_i}{2},$$

$$C_i = \frac{1}{4\pi}\left(2\ln\left|\frac{1+\cos\alpha_i}{2\cos\alpha_i}\right| + \cos\alpha_i - 1\right),$$

$$\mathbf{D}_i = \frac{1}{8\pi}\left[-\frac{(1-\cos\alpha_i)(7-\cos\alpha_i)}{\sin\alpha_i} + 3\ln\left|\frac{1+\sin\alpha_i}{\cos\alpha_i}\right|\right],$$

and $$\tan\alpha_i = \frac{r}{u_i z} \qquad (i = 1, 2, 3);$$

$u_3 = \sqrt{C_{66}/C_{44}}$; u_1 and u_2 are the roots of the following characteristic equation:

$$u^4 - su^2 + q = 0 \quad (9)$$

where $s = [C_{11}C_{33} - C_{13}(C_{13}+2C_{44})]/(C_{33}C_{44})$, $q = C_{11}/C_{33}$. If the strain energy is assumed positively definite in the medium [53], the root of Equation (9), u_1 and u_2 are restricted to the following three cases:

β (deg.)	Increment in a	β (deg.)	Increment in a	β (deg.)	Increment in a	β (deg.)	Increment in a	β (deg.)	Increment in a
0		0		0		0		0	
	1		1/2		1/4		1/6		1/8
90		30		14.48		9.59		7.18	
	-1		1/2		1/4		1/6		1/8
180		90		30		19.47		14.48	
			-1/2		1/4		1/6		1/8
		150		48.59		30		22.02	
			-1/2		1/4		1/6		1/8
		180		90		41.81		30	
					-1/4		1/6		1/8
				131.41		56.44		38.68	
					-1/4		1/6		1/8
				150		90		48.59	
					-1/4		-1/6		1/8
				165.52		123.56		61.04	
					-1/4		-1/6		1/8
				180		138.19		90	
							-1/6		-1/8
						150		118.96	
							-1/6		-1/8
						160.53		131.41	
							-1/6		-1/8
						170.41		141.32	
							-1/6		-1/8
						180		150	
									-1/8
								157.98	
									-1/8
								165.52	
									-1/8
								172.82	
									-1/8
								180	

For β between 0 and -180, the increment in a is the same as above.

Case 1. When $s^2-4q>0$,

$$u_{1,2}=\pm\sqrt{\frac{s\pm\sqrt{s^2-4q}}{2}}$$

are two real distinct roots.

Case 2. When $s^2-4q=0$,

$$u_{1,2}=\pm\sqrt{\frac{s}{2}},\ \pm\sqrt{\frac{s}{2}}$$

are real double roots (i.e., complete isotropy).

Case 3. When $s^2-4q<0$,

$$u_1=\frac{\sqrt{s+2\sqrt{q}}}{2}-i\frac{\sqrt{-s+2\sqrt{q}}}{2}=\gamma-i\delta,\qquad u_2=\gamma+i\delta$$

are two conjugate complex roots (where symbol γ cannot be equal to zero [1]);

Using engineering elastic constants, the following criterion can distinguish the root type of Equation (9).

$$\left(\frac{G}{G'}\right)^2(1+\upsilon)-\left(\frac{E}{E'}\right)\left[1-\upsilon+\left(\frac{E}{G'}\right)\upsilon'-2\left(\frac{E}{E'}\right)\upsilon'2\right]\begin{cases}>0, & \text{for case 1}\\ =0, & \text{for case 2}\\ <0, & \text{for case 3}\end{cases}\tag{10}$$

Table 3. Values of A_i with various r/u_iz

A_i	Increment in A_i	r/u_iz	No. of segments in 1/4 circle	The numbered block in Fig. 8
0	0	0	0	
0.001	0.001	0.446	1	1
0.003	0.002	0.686	2	2
0.005	0.002	0.856	2	
0.007	0.002	1.005	2	
0.009	0.002	1.143	2	
0.011	0.002	1.276	2	
0.015	0.004	1.537	4	4
0.019	0.004	1.803	4	
0.023	0.004	2.081	4	
0.027	0.004	2.376	4	
0.031	0.004	2.693	4	
0.037	0.006	3.217	6	6
0.043	0.006	3.812	6	
0.049	0.006	4.492	6	
0.055	0.006	5.274	6	
0.061	0.006	6.176	6	
0.067	0.006	7.218	6	
0.075	0.008	8.867	8	***** * 8 * *****
0.083	0.008	10.876	8	
⋮	⋮	⋮	⋮	
∞	∞	∞	∞	

Gerrard [54] and Amadei *et al.* [53] demonstrated that, for most transversely isotropic rocks, E/E' and G/G' are within 1 and 3; the Poisson's ratios υ and υ' are within between 0.15 and 0.35. Figure 2 presents the distribution of the three types of the characteristic roots for transversely isotropic rocks with E/E' and G/G' ranging from 1 to 3. This figure reveals that approximately two thirds of transversely isotropic rocks belong to case 1 (i.e., two real distinct roots). The results shown in Fig. 2 are compatible with available, published data [46–51] listed in Table 1 where all but one transversely isotropic rock belong to case 1.

Preparation of the influence charts

The new influence charts include an index scale representing the depth of the desired point, and numbers of concentric circles and radial lines. A unit block, except for those adjacent to the point C, is formed by two radial lines and two concentric circle arcs. $[\sigma]^C$ depends on the geometry of the loaded sector as described in Equations (3)–(8). The geometry is defined by a set of coefficients a, b, c, d, e, f, g, $\mathbf{A}_i$, $\mathbf{B}_i$, $\mathbf{C}_i$ and $\mathbf{D}_i$. The values of a, b, c, d, e, f and g depend on the central angle β. The coefficients $\mathbf{A}_i$, $\mathbf{B}_i$, $\mathbf{C}_i$ and $\mathbf{D}_i$ relate to the ratio of r/u_iz. The value of c is positive regardless of the value of β. The others (i.e. a, b, d, e, f and g) can be either positive or negative. For a given depth u_iz, the values of $\mathbf{A}_i$, $\mathbf{B}_i$, $\mathbf{C}_i$ and $\mathbf{D}_i$ depend only on r, and $\mathbf{A}_1=\mathbf{A}_2=\mathbf{A}_3$, $\mathbf{B}_1=\mathbf{B}_2=\mathbf{B}_3$, and so on. Charts for $a\mathbf{A}_i$, $b\mathbf{A}_i$, $c\mathbf{B}_i$, $d\mathbf{C}_i$, $e\mathbf{C}_i$, $f\mathbf{D}_i$ and $g\mathbf{D}_i$ are required for estimating $[\sigma]^C$ in a half-space graphically. Considering the symmetric properties of triangular functions, the charts for $a\mathbf{A}_i$ and $b\mathbf{A}_i$ are identical, except that the x- and y-axes are exchanged. The same is true for $f\mathbf{D}_i$ and $g\mathbf{D}_i$. Consequently, only five independent charts (i.e. $a\mathbf{A}_i$, $c\mathbf{B}_i$, $d\mathbf{C}_i$, $e\mathbf{C}_i$, $f\mathbf{D}_i$) are needed for computing $[\sigma]^C$. Figures 3–7 depict the influence charts of $a\mathbf{A}_i$, $c\mathbf{B}_i$, $d\mathbf{C}_i$, $e\mathbf{C}_i$, $f\mathbf{D}_i$, respectively. The index length of depth u_iz in these figures is set to 1.3 cm. The calculated r is symmetrical with respect to the origin O, therefore, only one quarter of the charts is drawn. The sign " $-$ " in the figures indicates that the values of a,

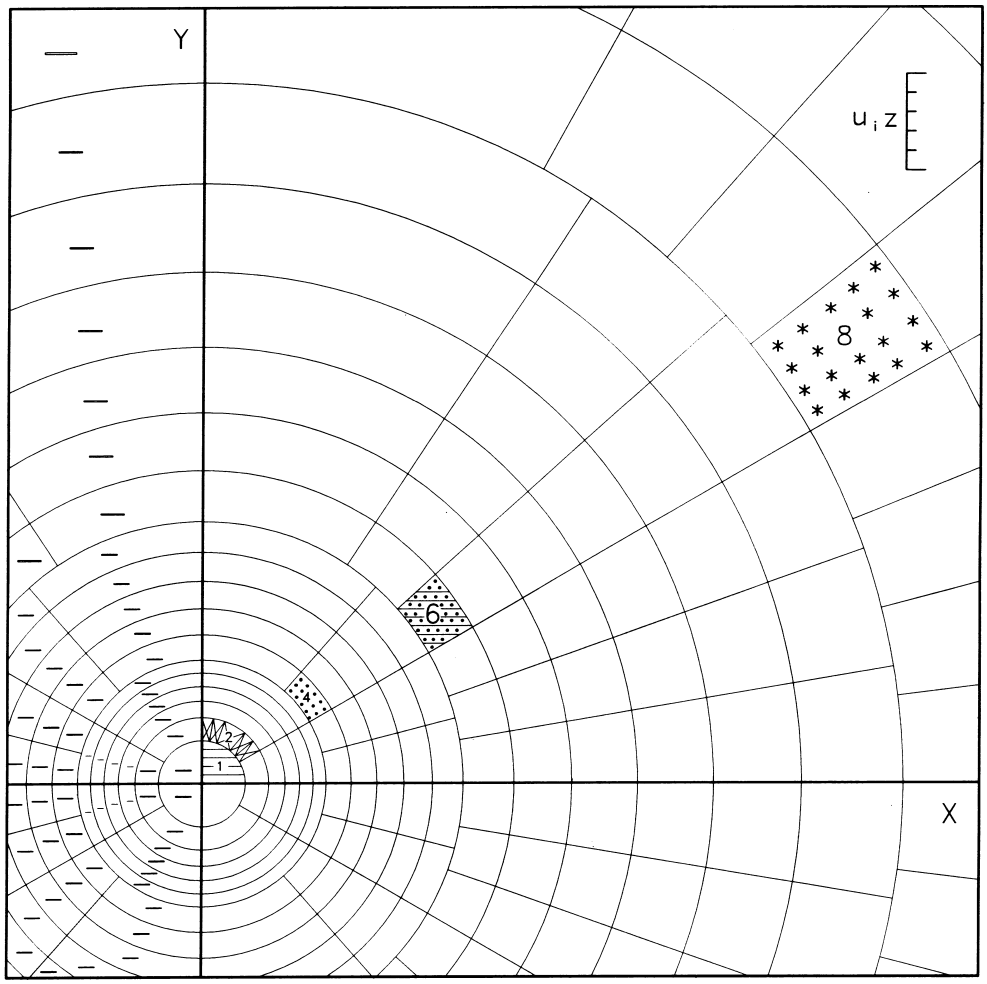

Fig. 8. The example of construction the influence chart for $a\mathbf{A}_i$.

b, d, e, f and g are negative. The influence value is negative for blocks with a " $-$ " sign.

To explain the construction of the influence charts, details of the preparation for $a\mathbf{A}_i$ chart are described below.

Considering a unit load intensity, the values of a (as a function of β) and $\mathbf{A}_i$ (as a function of $r/u_i z$) are calculated and listed in Tables 2–3. Table 2 shows increment of a in the first quadrant, the increment value of a is negative when the blocks locate in the second and third quadrants. $\mathbf{A}_i$ increases with $r/u_i z$ as shown in Table 3. For a given value of a with respect to β, the increment value of $\mathbf{A}_i$, 0.001, 0.002, 0.004, 0.006, 0.008, etc., is selected for the first, second, third, fourth, fifth, etc., ring group of the area formed by two adjacent concentric circles. The corresponding values of $r/u_i z$ for the circles are listed in Table 3. Combining the numerical values of a and $\mathbf{A}_i$, the radial lines and the concentric circles are drawn so that $a\mathbf{A}_i$ for all blocks in the chart is 0.001. For example, with specific values of β and $r/u_i z$ (the value of $a\mathbf{A}_i$ being 0.001 at the shaded area), the blocks numbered 1, 2, 4, 6, 8 in Fig. 8 are determined. The five independent charts are constructed according to the same unit length $u_i z$.

For a medium with conjugate complex roots of its characteristic equation (Equation (9)), the value of $u_i z$ is a complex variable and the influence charts cannot be drawn in this manner. For case 3 material, the preparation of influence charts requires elastic constants as a prior and $u_i z$ being replaced by z. It means that the charts prepared for case 3 material are valid only for a particular medium. Appendix A illustrates the method for constructing the influence charts and procedure to calculate vertical stress in a half-space for case 3 material.

PROCEDURE FOR USING THE INFLUENCE CHARTS

The influence charts provide an estimate of the six components of $[\sigma]^C$ at a point in the half-space subjected to three-dimensional surface loads with arbitrary shapes. A detailed procedure for establishing the charts and their applications is described as follows:

(1) Identify the type of rock (i.e. isotropic, transversely isotropic, orthotropic or generally anisotropic). If the rock is isotropic, the desired stresses can be computed using the Newmark's charts [38]. If the rock is orthotropic or generally anisotropic, there are no influence charts available.

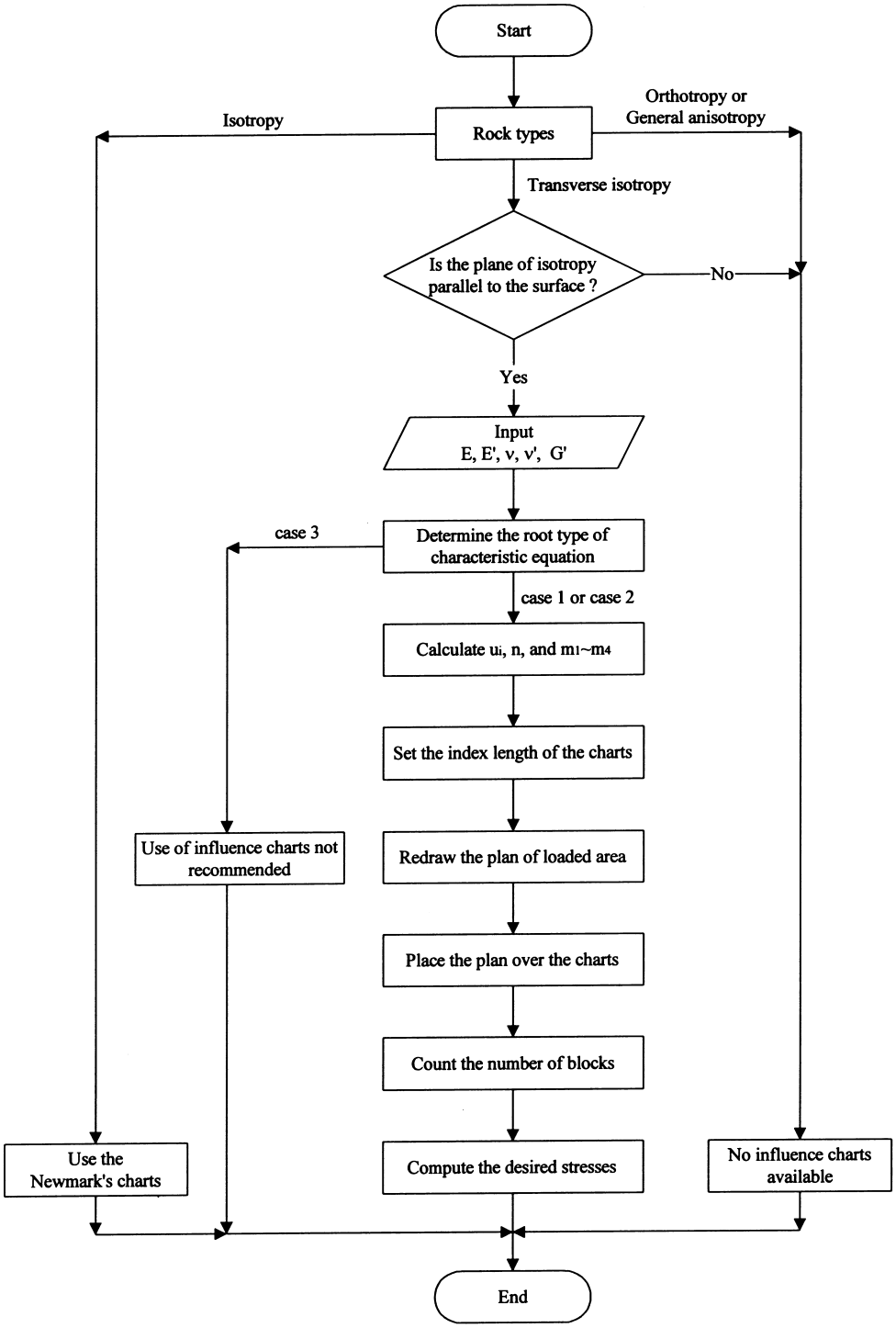

Fig. 9. Flow chart for computing the stresses induced by irregular loading shapes using influence charts.

(2) Verify if the planes of isotropy are parallel to the surface. The influence charts reported herein are applicable only if the planes of isotropy are parallel to the surface.

(3) Determine the root type of characteristic equation [i.e. case 1, 2 or 3, in Equation (10)] for the half-space. Continue to step (4) through (9) if the root type is case 1 or case 2. If the root type is case 3, the influence charts will have to be prepared individually and the following steps do not apply.

(4) Calculate the characteristic root u_i (i = 1, 2, 3) from Equation (9), functions n and $m_1 \sim m_4$.

(5). Compute $u_i z$ (i = 1, 2, 3) and use that as the unit length to scale the loaded areas on each influence chart (shown at the right hand corner in Figs 3–7).

(6) Redraw the plan of the loaded area using the scale obtained in step (5). A transparent paper is recommended.

(7) Place the plan of the loaded area plotted in step (6) on the influence charts. The point at which the

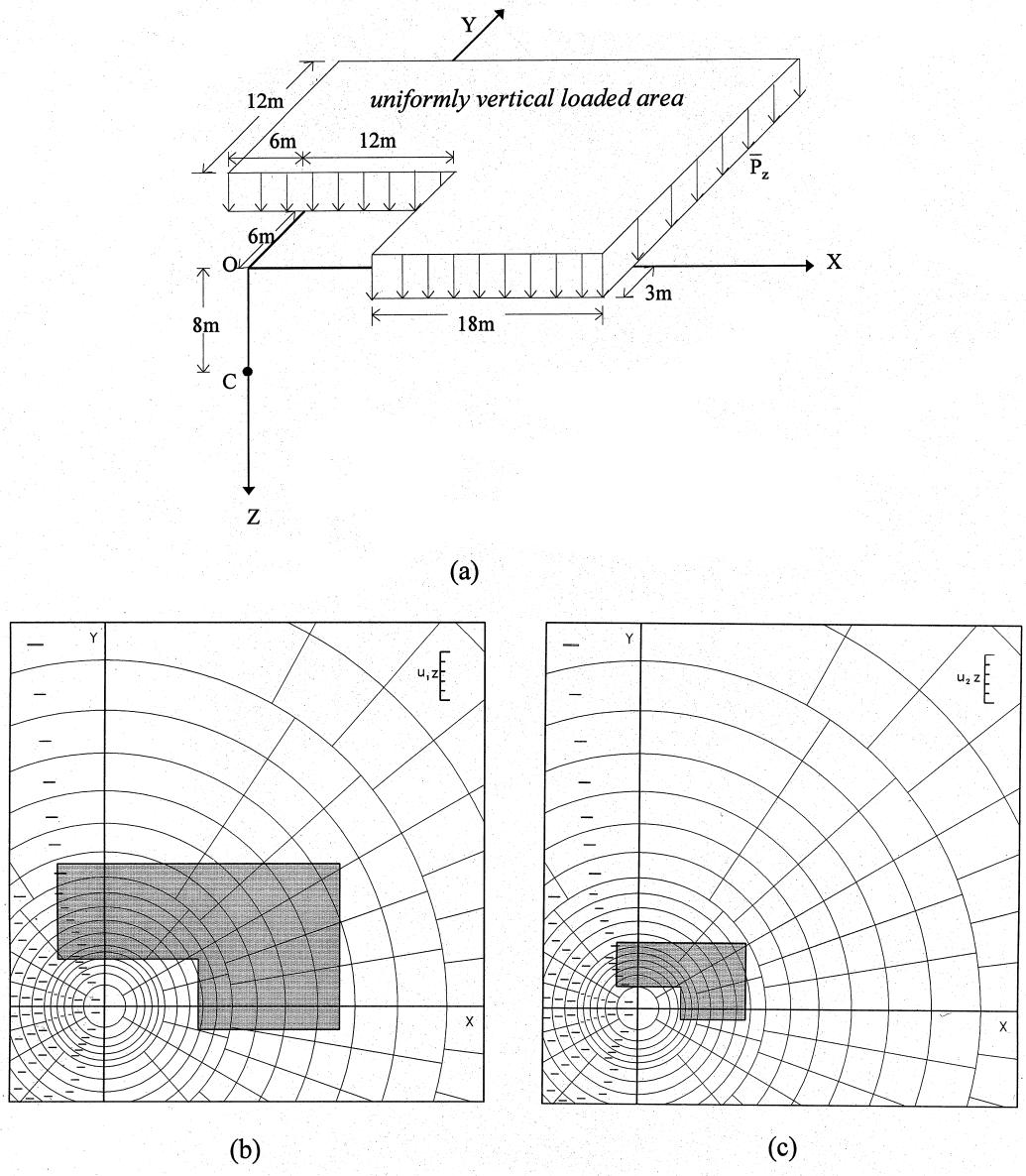

Fig. 10. (a) Plan of loaded area acting on the surface. (b) The blocks covered by the plan of the loaded area for $a\mathbf{A}_1$. (c) The blocks covered by the plan of the loaded area for $a\mathbf{A}_2$.

Table 4. The calculated procedures and results for transversely isotropic rocks subjected to the loaded area of Fig. 10(a)

	Coefficients associated with Eqns (11)–(16)												
	$4u_2m_1/u_1 = 5.591$			$2m_2/u_2 = 3.686$	$2m_1/u_1 = 1.686$	$u_2m_3 = 1.391$	$u_1m_4 = 2.120$	$u_2^*(2m_2\text{-}m_3) = 0.728$		$u_1^*(2m_1\text{-}m_4) = 2.513$	$u_2m_3 = 1.391$	$u_1m_4 = 2.120$	
Number of blocks on Figs 3–7	$a\mathbf{A}_1$ 32	$a\mathbf{A}_2$ 20	$b\mathbf{A}_1$ 43	$b\mathbf{A}_2$ 19	$c\mathbf{B}_1$ 61	$c\mathbf{B}_2$ 60	$d\mathbf{C}_1$ 58	$d\mathbf{C}_2$ 23	$c\mathbf{B}_1$ 61	$c\mathbf{B}_2$ 60	$e\mathbf{C}_1$ 2	$e\mathbf{C}_2$ 10	
Influence value	0.001				$\sigma_{zz}^C/\bar{P}_z$		$\tau_{xy}^C/\bar{P}_z$			$\sigma_{xx}^C/\bar{P}_z$ and $\sigma_{yy}^C/\bar{P}_z$			
Normalized stresses	$\tau_{xz}^C/\bar{P}_z$ Equation (15)		$\tau_{yz}^C/\bar{P}_z$ Equation (14)		Equation (13)		Equation (16)			Equation (11) and Equation (12)			
Calculated results	0.0671		0.1342		0.1237		0.0319		0.0879			0.1248	
Analytical results	0.0701		0.1302		0.1219		0.0308		0.0902			0.1287	
Error percent (%)	4.3		3.1		1.5		3.6		2.5			3.0	

Five elastic constants: $E = 51.8$ GPa, $E' = 32.2$ GPa, $\nu = 0.19$, $\nu' = 0.18$, $G' = 13.3$ GPa. Elastic constants: $C_{11} = 58.5$ GPa, $C_{13} = 13.2$ GPa, $C_{33} = 37.0$ GPa, $C_{44} = 13.3$ GPa, $C_{66} = 21.8$ GPa. Characteristic roots: $u_1 = 0.758$, $u_2 = 1.658$, $u_3 = 1.279$. Related coefficients: $n = 2.527$, $m_1 = 0.639$, $m_2 = 3.056$, $m_3 = 0.839$, $m_4 = 2.797$.

stresses are desired should be placed over the center of the circles on these charts.

(8) Count the number of blocks on the influence charts covered by the plan of the loaded area.

(9) Compute the stress tensor using Equations (3)–(8) based on functions n, $m_1 \sim m_4$ [from step (4)] and the number of blocks covered by plan of the loaded area [from step (8)].

Figure 9 presents a flow chart that illustrates the use of the influence charts. Although the charts are proposed for uniform loads, the stress induced by non-uniform loads can be estimated by dividing the entire loading area into several sub-areas, each with an approximately uniform load.

DEMONSTRATION AND VERIFICATION

To validate the proposed stress influence charts and demonstrate its capabilities, an example is presented in this section. The half-space is subjected to a uniform normal load ($\bar{P}_z$) on the horizontal surface with a loading area shown in Fig. 10(a). The point (i.e. point C) where $[\sigma]^C$ is to be computed is at 8 meters below point O. The half-space is transversely isotropic (argillite) and the planes of transverse isotropy are parallel to the horizontal surface. The five elastic constants are $E = 51.8$ GPa, $E' = 32.2$ GPa, $\upsilon = 0.19$, $\upsilon' = 0.18$, and $G' = 13.3$ GPa [48]. From Equation (10), the medium belongs to case 1 with two real distinct roots. Equations (3)–(8) are rewritten as:

$$\frac{\sigma_{xx}^C}{\bar{P}_z} = -u_2(2m_1 - m_3)\cdot c\mathbf{B}_1 + u_1(2m_2 - m_4)\cdot c\mathbf{B}_2 + u_2m_3\cdot e\mathbf{C}_1 - u_1m_4\cdot e\mathbf{C}_2 \tag{11}$$

$$\frac{\sigma_{yy}^C}{\bar{P}_z} = -u_2(2m_1 - m_3)\cdot c\mathbf{B}_1 + u_1(2m_2 - m_4)\cdot c\mathbf{B}_2 - u_2m_3\cdot e\mathbf{C}_1 + u_1m_4\cdot e\mathbf{C}_2 \tag{12}$$

$$\frac{\sigma_{zz}^C}{\bar{P}_z} = \frac{2m_2}{u_2}\cdot c\mathbf{B}_1 - \frac{2m_1}{u_1}c\mathbf{B}_2 \tag{13}$$

$$\frac{\tau_{yz}^C}{\bar{P}_z} = \frac{4u_2m_1}{u_1}(b\mathbf{A}_1 - b\mathbf{A}_2) \tag{14}$$

$$\frac{\tau_{xz}^C}{\bar{P}_z} = \frac{4u_2m_1}{u_1}(a\mathbf{A}_1 - a\mathbf{A}_2) \tag{15}$$

$$\frac{\tau_{xy}^C}{\bar{P}_z} = u_2m_3\cdot d\mathbf{C}_1 - u_1m_4\cdot d\mathbf{C}_2 \tag{16}$$

Equations (11)–(16) indicate that, knowing the elastic constants, u_i and $m_1 \sim m_4$, one or two independent in-

fluence charts would be enough to determine the six components of $[\sigma]^C$. For example, influence charts for $c\mathbf{B}_i$ and $e\mathbf{C}_i$ can be used to compute σ_{xx}^C and σ_{yy}^C; influence chart $c\mathbf{B}_i$ is enough for calculating σ_{zz}^C; τ_{yz}^C, τ_{xz}^C, τ_{xy}^C, and can be estimated from the influence chart of $b\mathbf{A}_i$, $a\mathbf{A}_i$, and $d\mathbf{C}_i$, respectively. For illustrative purpose, the procedure of calculating $\tau_{xz}^C/\bar{P}_z$ is described as follows:

(1) Calculate the characteristic root u_i (i = 1, 2, 3) from Equation (9), functions n and $m_1 \sim m_4$. The results are given in Table 4.

(2) Set the unit length as: $u_1 z = 6.064$, $u_2 z = 13.264$ for $a\mathbf{A}_1$ and $a\mathbf{A}_2$, respectively.

(3) Redraw the plan of the loaded area using the scales obtained in step (2) on transparent papers (for $a\mathbf{A}_1$ and $a\mathbf{A}_2$).

(4) Place the transparent papers prepared in step (3) on the influence chart ($a\mathbf{A}_i$). Point C should be placed over the center of the chart. Figures 10(b) and (c) demonstrate the procedure for overlapping planes of the loaded area on the chart for $a\mathbf{A}_1$ and $a\mathbf{A}_2$, respectively.

(5) Count the number of blocks on Fig. 10(b) and (c) covered by the loaded area. The numbers of blocks, rounded to the nearest integer, is 32 in Fig. 10(b) and 20 in Fig. 10(c).

(6) From Equation (15), the normalized shear stress ($\tau_{xz}^C/\bar{P}_z$) at point C is computed as:

$$\tau_{xz}^C/\bar{P}_z = 5.591 \times (32 - 20) \times 0.001 = 0.0671$$

Similarly, the other normalized stress components can be calculated and the results are shown in Table 4. Comparing the results with analytic solutions of Lin *et al.* [6] by superposition, the six stress components computed using the influence charts agree with the analytic results within 3%.

CONCLUSIONS

Based on the integration of closed-form solutions for a point load, a series of five influence charts have been developed to calculate the stress tensor within an elastic transversely isotropic half-space that is subjected to a surface load with an irregularly-shaped area. Following the idea of Newmark's charts for isotropic materials, the new influence charts consist of unit blocks. Each unit block is bounded by two adjacent radii and arcs, and contributes the same influence to the induced stress. In this article, the influence of each unit block is selected to be 0.001 of the surface load intensity. The stress at the point of interest is computed by counting the number of blocks covered by the plan of the loaded area drawn to a scale set by the material properties. The proposed influence charts are suitable for transversely isotropic materials with real roots of the characteristic equation. The new influence charts are easy to use and results are reasonably accurate. These charts offer a practical alternative to analytical and numerical solutions.

Acknowledgements—The research was funded by the National Science Council of R.O.C. under contract No. NSC 86-2621-E009-011. The authors would like to thank Professors Y. W. Pan and A. B. Huang for their valuable discussions during the work.

REFERENCES

1. Lekhnitskii, S. G., *Theory of Elasticity of an Anisotropic Elastic Body*. Holden-Day, San Francisco, 1963.
2. Pan, Y. C. and Chou, T. W., Green's function solutions for semi-infinite transversely isotropic materials. *Int. J. Eng. Sci.*, 1979, **17,** 545–551.
3. Liao, J. J. and Wang, C. D., Elastic solutions for a transversely isotropic half-space subjected to a point load. *Int. J. Numer. Anal. Methods Geomech.*, in press.
4. Anon, De spanningsverdeling in eenn homogeen anisotroop elastisch half medium. *L. G. M. Mededelingen*, 1960, **5**, 33–51.
5. Urena, R. D., Piquer, J. S., Muzas, F., and Saracho, J. M. S., Stress distribution in cross-anisotropic media. In *Proc. 1st ISRM Congr. Lisbon*, Vol. 1, 1966, pp. 313–317.
6. Lin, W., Kuo, C. H. and Keer, L. M., Analysis of a transversely isotropic half space under normal and tangential loadings. *J. Tribology ASME*, 1991, **113,** 335–338.
7. Piquer, J. S., Muzas, F., Urena, R. D. and Grajera, F., Foundations in cross-anisotropic ground. In *Proc. 1st ISRM Congr. Lisbon*, Vol. 1, 1966, pp. 531–536.
8. Barden, L., Stresses and displacements in a cross-anisotropic soil. *Geotechnique*, 1963, **13,** 198–210.
9. Gerrard, C. M. and Harrison, W. J., Circular loads applied to a cross-anisotropic half space. Technical Paper No. 8, CSIRO, 1970.
10. Nayak, M., Elastic settlement of a cross-anisotropic medium under axisymmetric loading. *Soils and Foundations*, 1973, **13,** 83–90.
11. Hooper, J. A., Elastic settlement of a circular raft in adhesive contact with a transversely isotropic medium. *Geotechnique*, 1975, **25,** 691–711.
12. Misra, B. and Sen, B. R., Stresses and displacements in granular materials due to surface load. *Int. J. Eng. Sci.*, 1975, **13,** 743–761.
13. Chowdhury, K.L ., On the axisymmetric Mindlin's problem for a semi-space of granular material. *Acta Mech.*, 1987, **66,** 145–160.
14. Hanson, M. T. and Puja, I. W., Love's circular patch problem revisited: closed form solutions for transverse isotropy and shear loading. *Q. Appl. Math.*, 1996, **54,** 359–384.
15. Quinlan, P. M., A Fourier integral approach to an aelotropic medium. Ph.D. thesis, California Institute of Technology, 1949.
16. Gazetas, G., Stresses and displacements in cross-anisotropic soils. *J. Geotech. Eng. Div. ASCE*, 1982, **108,** 532–553.
17. Gazetas, G., Axisymmetric parabolic loading of anisotropic half-space. *J. Geotech. Eng. Div. ASCE*, 1982, **108,** 654–660.
18. Hasegawa, H. and Watanabe, K., Green's functions for axisymmetric surface force problems of an elastic half space with transverse isotropy. *Jpn. Soc. Mech. Eng.*, 1995, **95,** 438–439.
19. Hanson, M. T. and Wang, Y., Concentrated ring loadings in a full space or half space: solutions for transverse isotropy and isotropy. *Int. J. Solids Struct.*, 1997, **34,** 1379–1418.
20. Sveklo, V. A., The action of a stamp on an elastic anisotropic half-space. *PMM*, 1970, **34,** 172–178.
21. Gladwell, G. M. L., Polynomial solutions for an ellipse on an anisotropic elastic half-space. *Q. J. Mech. Appl. Math.*, 1978, **31,** 251–260.
22. Wolf, K., Ausbreitung der kraft in der halbebene und in halbraum bei anisotropen material. *Z. Angew. Math. Mech.*, 1935, **15,** 249–254.
23. Bray, J., Unpublished notes. Imperial College, Royal School of Mines, London, 1977.
24. Hall, R. W., Traction problems on an elastic jointed rock half-space. *Rock Mech.*, 1979, **12,** 115–135.
25. Liao, J. J. and Amadei, B., Surface loading of anisotropic rock masses. *J. Geotech. Eng. Div. ASCE*, 1991, **117,** 1779–1800.
26. Vallabhan, C. V. G., A computer programme for stresses in clay under footings. *Ind. Concrete J.*, 1971, 253–257.

27. Uzan, J. and Sides, A., The effect of contact area shape and pressure distribution on multilayer systems response. *Transport. Res. Rec*., 1987, **1117,** 21–24.
28. Thompson, J. C., Lelievre, B., Beckie, R. D. and Negus, K. J., A simple procedure for computation of vertical soil stresses for surface regions of arbitrary shape and loading. *Can. Geotech. J*., 1987, **24,** 143–145.
29. Murti, V. and Wang, Y. C., Stress distribution underneath an arbitrary shaped foundation. UNICIV-R265, 1989.
30. Murti, V., Wang, Y. C., Sastra, H. and Chandrasekaran, V., Vertical stress distribution due to an arbitrarily shaped foundation using triangulation and an indirect method. *Comput. Struct*., 1990, **36,** 667–680.
31. Murti, V. and Wang, Y. C., Vertical stress distribution due to an arbitrarily shaped foundation using triangulation and an analytical expression for a triangular loaded region. *Int. J. Numer. Anal. Methods Geomech*., 1991, **15,** 51–60.
32. Sutcliffe, D. E. and Selvadurai, A. P. S., Computer adaptation of Newmark's charts. *Microcomput. Civ. Eng*., 1988, **3,** 257–264.
33. Pulmano, V. A., Murti, V. and Chiu, S. L. S., Vertical soil stresses under foundations of arbitrary shape and loading using parametric mapping. In *Proc. Asian Pacific Conf. on Computational Mech*., Rotterdam, Vol. 1, 1991, pp. 783–788.
34. Li, K. S., A simple procedure for calculating vertical soil stress due to an arbitrarily shaped foundation. *Geotechnique*, 1991, **41,** 467–469.
35. Li, K. S., Elastic solutions for arbitrarily shaped foundations. *J. Geotech. Eng. ASCE*, 1992, **118,** 938–942.
36. Burmister, D. M., Graphical distribution of vertical pressure beneath foundations. *Trans. Am. Soc. Civ. Eng*., 1938, **103,** 303–313.
37. Newmark, N. M., Discussion to graphical distribution of vertical pressure beneath foundations. *Trans. Am. Soc. Civ. Eng*., 1938, **103,** 321–324.
38. Newmark, N. M., Influence charts for computation of stresses in elastic foundations. *Eng. Expt. Station Bull*., 1942, **338,** 5–25.
39. Newmark, N. M., Influence charts for computation of vertical displacements in elastic foundations. *Eng. Expt. Station Bull*., 1947, **367,** 7–11.
40. Salas, J. A. J., Soil pressure computation: a modification of the Newmark's method. In *Proc. 2nd Int. Conf. on Soil Mech. Found. Engrg*., Rotterdam, Vol. 1, 1948, pp. 30–34.
41. Barber, E. S., *Public Roads*. June, 1965.
42. Barber, E. S., Discussion to an influence chart for vertical stress increase due to horizontal shear loadings. *High. Res. Rec*., 1966, **108,** 17–18.
43. Barksdale, R. and Harr, M. E., An influence chart for vertical stress increase due to horizontal shear loadings. *High. Res. Rec*., 1966, **108,** 1–16.
44. Huang, S. Y., Graphical solution for vertical stress distributions and settlement in soil due to uniformly applied vertical loads acting on a buried area. M.Sc. thesis, The Cooper Union for the Advancement of Science and Art, 1995.
45. Poulos, H. G., The use of the sector method for calculating stresses and displacements in an elastic mass. In *Proc. 5th Australia-New Zealand Conf. Soil Mech. Found. Eng*., 1967, pp. 198–204.
46. Pinto, J. L., Deformability of schistous rocks. In *Proc. 2nd ISRM Congr*., Vol. 1. Belgrade, Vol. 1, 1970, pp. 491–496.
47. Homand, F., Morel, E., Henry, J.-P., Cuxac, P. and Hammade, E., Characterization of the moduli of elasticity of an anisotropic rock using dynamic and static methods. *Int. J. Rock Mech. Min. Sci. Geomech. Abstr*., 1993, **30,** 527–535.
48. Liu, J. Y., Liao, J. J. and Wang, C. D., Deformability of transversely isotropic rocks. In *Proc. '94 Rock Eng. Symp. Taiwan*. The National Central University, Chungli, Taiwan, 1994, pp. 101–110 (in Chinese).
49. Amadei, B., Importance of anisotropy when estimating and measuring in situ stresses in rock. *Int. J. Rock Mech. Min. Sci. Geomech. Abstr*., 1996, **33,** 293–325.
50. Liao, J. J., Yang, M. T. and Hsieh, H. Y., Direct tensile behavior of a transversely isotropic rock. *Int. J. Rock Mech. Min. Sci*., 1997, **34,** 837–849.
51. Liao, J. J., Hu, T. B. and Chang, C. W., Determination of dynamic elastic constants of transversely isotropic rocks using a single cylindrical specimen. *Int. J. Rock Mech. Min. Sci*., 1997, **34,** 1045–1054.

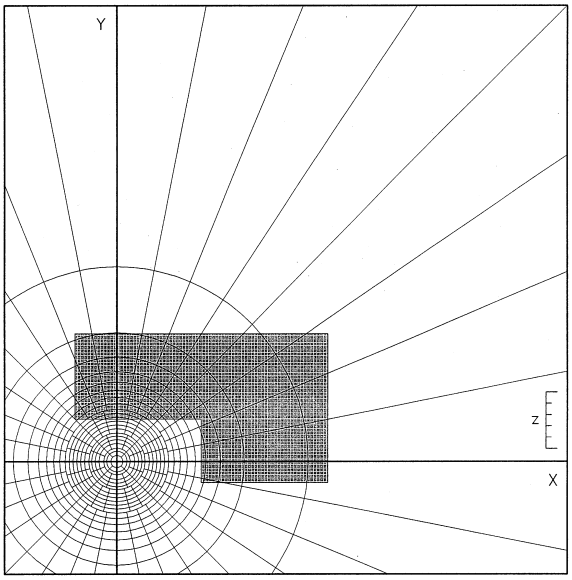

Fig. A1. Plan of loaded area on the influence chart for $c\mathbf{B}'$ (E = 50 GPa, E' = 25 GPa, G/G' = 1, ν = ν' = 0.25, influence value per block is 0.001).

52. Gradshteynn, I. S. and Ryzhik, I. M., *Tables of Integrals, Series, and Products*, 5th edn. Academic Press, San Diego, California, 1994.
53. Amadei, B., Savage, W. Z. and Swolfs, H. S., Gravitational stresses in anisotropic rock masses. *Int. J. Rock Mech. Min. Sci. Geomech. Abstr*., 1987, **24,** 5–14.
54. Gerrard, C. M., Background to mathematical modeling in geomechanics: The roles of fabric and stress history. In *Proc. Int. Symp. on Numerical Methods*. Karlsruhe, 1975, pp. 33–120.

APPENDIX A

To demonstrate the construction of influence charts and their applications for case 3, an example for evaluating vertical stress (σ_{zz}^C) in the elastic half-space, induced by a uniform normal load ($\bar{P}_z$) is illustrated. Say that $\boldsymbol{u}_1 = \boldsymbol{\gamma} - i\boldsymbol{\delta}$, $\boldsymbol{u}_2 = \boldsymbol{\gamma} + i\boldsymbol{\delta}$, the normalized vertical stress ($\sigma_{zz}^C/\bar{P}_z$) can be expressed in terms of the central angle $\boldsymbol{\beta}$ and a depth ratio $\boldsymbol{r}/\boldsymbol{z}$ as follows:

$$\frac{\sigma_{zz}^C}{\bar{P}_z} = \frac{2m_2}{u_2} \cdot c\mathbf{B}_1 - \frac{2m_1}{u_1} c\mathbf{B}_2 = 2c\mathbf{B}' \tag{A.1}$$

where

$$c = \frac{\beta}{2\pi}, \qquad \mathbf{B}' = \left[1 - \frac{j(\gamma^2 + \delta^2)}{h\delta}\right]/2,$$

$$h = \sqrt{\left[\left(\frac{r}{z}\right)^2 + \gamma^2 - \delta^2\right]^2 + 4\gamma^2\delta^2},$$

$$j = \frac{1}{\sqrt{2}}\sqrt{h\left(\frac{r}{z}\right)^2 - \gamma^2 + \delta^2}$$

In establishing the chart of $c\mathbf{B}'$, the elastic constants of the medium are involved. Assuming that the elastic constants are E = 50 GPa, E' = 25 GPa (E/E' = 2), G/G' = 1, and υ = υ' = 0.25, and solving Equation (9), the characteristic roots are complex and the values of symbol γ and δ are 1.0082 and 0.5914, respectively. The rest of the procedure in setting up $c\mathbf{B}'$ chart is similar to those of $a\mathbf{A}_i$, $c\mathbf{B}_i$, $d\mathbf{C}_i$, $e\mathbf{C}_i$, and $f\mathbf{D}_i$. Figure A1 shows the influence chart of $c\mathbf{B}'$. For a uniform load as shown in Fig. 10(a) and using z as the scale (right hand corner of Fig. 11), one can redraw the plan of the loaded area. The number of blocks covered by the loaded area is approximately 75. Using Equation (A.1), the normalized vertical stress $\sigma_{zz}^C/\bar{P}_z$ is equal to 0.15 ($= 2 \times 75 \times 0.001$). The result is very close to the exact solution (0.1535) of Lin *et al.* [6] by superposition.

Accepted for publication 12 February 1998